Thin Solid Films 603 (2016) 165–172

Contents lists available at ScienceDirect

Thin Solid Films

journal homepage: www.elsevier.com/locate/tsf

A benzodithiophene–thienothiophene derivative with cyano acrylate side chain: A novel donor polymer with deep HOMO level for p–n heterojunction solar cells

Yu Jin Kim [b,*,1], Eun Soo Ahn [a,1], Moon Chan Hwang [c], Chan Eon Park [b], Yun-Hi Kim [a]

[a] Department of Chemistry & RIGET, Gyeongsang National University, Jin-ju 660-701, Republic of Korea
[b] POSTECH Organic Electronics Laboratory, Department of Chemical Engineering, Pohang University of Science and Technology, Pohang 790-784, Republic of Korea
[c] School of Materials Science & Engineering and Engineering Research Institute (ERI), Gyeongsang National University, Jin-ju 660-701, Republic of Korea

ARTICLE INFO

Article history:
Received 2 October 2015
Received in revised form 22 December 2015
Accepted 3 February 2016
Available online 5 February 2016

Keywords:
Organic solar cell
Bulk heterojunction solar cell
Conjugated donor polymer
Power conversion efficiency
Open circuit voltage

ABSTRACT

A new promising benzodithiophene and thienothiophene-based copolymer with cyano acrylate side chain, BDT8TT, has been designed and synthesized for efficient bulk heterojunction solar cells. The copolymer shows good solubility and film-forming ability combining with excellent thermal stability. Furthermore, BDT8TT displays a broad absorption in the near-IR region (from 300 to 1000 nm). Specially, this conjugated polymer exhibits quite high open circuit voltage by a highly deep-lying HOMO level at −5.76 eV. Good power conversion efficiencies are demonstrated in solar cell studies; the polymer solar cell was fabricated from the blend of the polymer as a donor and $PC_{71}BM$ as an acceptor without annealing and any additives.

© 2016 Elsevier B.V. All rights reserved.

1. Introduction

Organic photovoltaics (OPVs) based on the bulk heterojunction (BHJ) active blends consisting of electron donating polymers and electron accepting fullerene derivatives have attracted significant interest due to their low-cost fabrication, light weight devices, and mechanically flexibility [1–4]. Caused by the rapid progress of the development of new conjugated polymers, the power conversion efficiency (PCE) of BHJ solar cells has now reached around 10% [5–6]. Indeed, to improve the PCE further, considerable efforts and investigations have been made to increase the open circuit voltage (Voc), short circuit current (Jsc), and fill factors (FF) of the OPVs [7–11]. So far, considering thousands of publications in the OPV field, the majority of important achievements are more or less related to the use of novel donor–acceptor (D–A) conjugated polymers. Therefore, the molecular design of D–A polymers has become a very important topic with considerable further promise.

From the point of view of the molecular design of D–A polymers, in previous work, we designed and synthesized a conjugated polymer, CNTT, with a unique structure composed of a main chain donor (thiophene and thienothiophene units) and a side chain acceptor (cyanoacrylate group), and by the use of this novel concept, conjugated polymers, light harvesting, and photovoltaic properties can be improved distinctly [12]. Although these copolymers demonstrate great characteristics as OPVs, one drawback of the CNTT system is its quite low Voc (i.e., the CNTT device exhibits a low Voc value, 0.35 V). Sometimes the introduction of strong electron-donating moiety in the polymer backbone is not very efficient to enhance the Voc, i.e. when thiophene derivative units were introduced on the polymer chain, the highest occupied molecular orbital (HOMO) levels of the corresponding copolymer can be elevated by 0.2–0.3 eV, and as reflected in photovoltaic behaviors, the Voc of the polymer solar cells can significantly be reduced by 0.1–0.3 V [13–15].

Therefore, we newly designed and synthesized a D–A conjugated polymer with established structure, poly(4,8-bis(octyloxy)benzo[1,2-b:4,5-b′]dithiophene-co-2-octyldodecyl (Z)-2-cyano-3-(thieno[3,4-b]thiophen-2-yl)acrylate) (BDT8TT). The benzodithiophene (BDT) unit was selected to replace the thiophene moiety to reduce the HOMO energy level of the polymer. Introducing the BDT unit in semiconducting polymers is effective for shifting the frontier molecular orbital energy levels down via the weak electron donating nature [16–17]. Indeed, incorporating BDT moiety in the conjugated BDT8TT polymer, an efficient p–n heterojunction solar cell with a boosted Voc of 0.77 V by the extremely deep-lying HOMO levels of −5.76 eV is achieved.

* Corresponding author.
E-mail address: youjinfall@postech.ac.kr (Y.J. Kim).
[1] Yu Jin Kim and Eun Soo Ahn contributed equally to this work.

http://dx.doi.org/10.1016/j.tsf.2016.02.004
0040-6090/© 2016 Elsevier B.V. All rights reserved.

2. Experimental

2.1. Materials

All reagents from commercial sources were used without further purification. Tetrahydrofuran (THF), acetonitrile (CH_3CN), *N,N*-dimethylformamide (DMF), ethyl ether and 1,2-dichloromethane (DCM) were purchased from Aldrich and were purified by passage under a N_2 atmosphere. Catalyst was purchased from Umicore.

2.2. Synthesis

2.2.1. Synthesis of 4,8-bis(octyloxy)benzo[1,2-b:4,5-b′]dithiophene (1)

Under the protection of nitrogen, benzo[1,2-b:4,5-b′]dithiophene-4,8-dione (6 g, 26.7 mmol), $Na_2S_2O_4$ (14 g, 80.2 mmol), and tetrabutylammonium bromide (19 g, 58.8 mmol) in water (90 mL) were well mixed for 10 min. THF (120 mL) was then added, along with NaOH (16 g). The mixture was then stirred for 2 h at room temperature while purging with nitrogen. 1-Bromooctane (15.5 g, 80.2 mmol) was added and the mixture stirred at 80 °C overnight. The solution was then diluted with water and extracted with diethyl ether. The organic extract was dried over $MgSO_4$ and the solvent was removed. Further purification was carried out by column chromatography on silica gel using hexane as eluent. Yield: 11 g (91.66%) ^{1}H NMR (300 MHz, $CDCl_3$, ppm): δ = 9.95 (s, 1 H), 8.13 (d. 1 H), 7.37 (d, 1 H). ^{13}C NMR (75 MHz, $CDCl_3$, ppm): δ = 185.3, 145.6, 139.2, 128.4, 111.7. EI, MS *m/z*: 191 (M+).

2.2.2. Synthesis of (4,8-bis(octyloxy)benzo[1,2-b:4,5-b′]dithiophene-2,6-diyl)bis(trimethylstannane) (2)

n-Butyllithium (3.9 mL, 9.8 mmol, 2.5 M in hexane) was added to a solution of compound **(1)** (2 g, 5.4 mmol) in THF (30 mL) at 0 °C in a nitrogen-purged flask. The mixture was then warmed to 50 °C and stirred for 2 h at ambient temperature. Subsequently, trimetyltin chloride (2.1 g, 10.3 mmol) was added and the mixture stirred for an additional 3 h. It was then poured into ice/water, extracted with diethyl ether, and the combined organic phases concentrated to obtain the crude product. Further purification was carried out by column chromatography on alumina silica gel by using hexane as eluent. Yield: 2.07 g (60.0%) ^{1}H NMR (300 MHz, $CDCl_3$, ppm): δ = 9.95 (s, 1 H), 8.13 (d. 1 H), 7.37 (d, 1 H). ^{13}C NMR (75 MHz, $CDCl_3$, ppm): δ = 185.3, 145.6, 139.2, 128.4, 111.7. EI, MS *m/z*: 191(M+).

2.2.3. Synthesis of 4,6-dibromothieno[3,4-b]thiophene-2-carbaldehyde (3)

The synthetic details of starting (thieno[3,4-b]thiophene-2-carbaldehyde) can be found in the previous report [18].

A solution of thieno[3,4-b]thiophene-2-carbaldehyde (5 g, 29.71 mmol) in $CHCl_3$ and AcOH mixture(1:1) protected from light was cooled to 0 °C. *N*-Bromosuccinimide (2 g, 7.42 mmol) was added in small portion over 15 min, and then the reaction was stirred overnight. The organic layer was dried over anhydrous $MgSO_4$, and the solvent was removed. The residue was purified by column chromatography and purified crystallization from MC: petroleum ether (1:1) to yield compound 7 as a needle shaped brown solid. Yield: 8.75 g (70%) ^{1}H NMR (300 MHz, $CDCl_3$, ppm): δ = 9.99 (s, 1 H), 7.86 (s, 1 H).

2.2.4. Synthesis of 2-octyldodecyl (Z)-2-cyano-3-(4,6-dibromothieno[3,4-b]thiophen-2-yl)acrylate (4)

Under the protection of nitrogen, 4,6-dibromothieno[3,4-b]thiophene-2-carbaldehyde (1 g, 3.06 mmol), 2-octyldodecyl 2-cyanoacetate (1.68 g, 4.60 mmol), piperidine (0.28 g, 3.37 mmol), ethanol (2 mL) and CH_3CN (20 mL) was added and refluxed for 3 h. And then cooled down to room temperature. The solution was then diluted with water and extracted with chloroform. The organic extract was dried over $MgSO_4$ and the solvent was removed. Further purification was carried out by column chromatography on silica gel using n-hexane:ethyl acetate (10:1). Yield: 1.05 g (51.2%) ^{1}H NMR (300 MHz, $CDCl_3$, ppm): δ = 7.42 (s, 1 H), 7.20 (s. 1 H), 3.08 (t, 2 H), 1.82 (t, 1 H), 1.28 (m, 31 H), 0.90 (t, 6 H); FT-IR (KBr) (cm^{-1}): 3010 (aromatic), 2860–2780 (aliphatic, C—H), 2230–2252 (C≡N), 1510–2595 (aromatic, C═C), 809 (aliphatic, C—S).

2.2.5. Synthesis of poly(4,8-bis(octyloxy)benzo[1,2-b:4,5-b′]dithiophene-co-2-octyldodecyl (Z)-2-cyano-3-(thieno[3,4-b]thiophen-2-yl)acrylate) (BDT8TT)

Compound **(2)** (0.573 g, 0.742 mmol) and compound (**4**) (0.5 g, 0.742 mol) were dissolved dry chlorobenzene (5 mL). Then, $Pd_2(dba)_3$ (0.011 g, 0.0148 mmol) and P-(o-tol)$_3$ (0.039 g, 0.0579 mmol) were added and the reaction mixture was stirred at 110 °C under nitrogen atmosphere for 48 h. The polymer was purified by precipitation in methanol, filtered and washed on soxhlet apparatus with methanol, acetone, n-hexane, and chloroform. The chloroform fraction was evaporated under reduced pressure and the polymer was precipitated in methanol, filtered, and finally dried under high vacuum. Yield: 0.77 g (72.1%) ^{1}H NMR (500 MHz, $CDCl_3$, ppm): δ = 8.75–7.86 (3 H, br), 4.88–3.63 (34 H, br), 2.70–0.105 (38 H, br). Element Anal. $C_{56}H_{81}NO_4S_4$, Cal: C, 70.03; H, 8.50; N, 1.46; S, 13.35; Found: C, 69.07; H, 8.13; N, 1.51; S, 13.87.

2.3. General instruments

The ^{1}H-NMR and ^{13}C-NMR spectra were measured by a Bruker Advance-300 spectrometer. HR mass spectra were recorded by JMS 700 mstation. Fourier transform infrared spectroscopy (FT-IR) was performed on a NICOLET 6700 (Thermo electron corporation). The molecular weight and polydispersity index (PDI) of the synthesized copolymer were determined by gel permeation chromatography (GPC) using a polystyrene standard. GPC was conducted using water as the moving phase in a high-pressure GPC assembly using a Model M515 pump with u-Styragel columns of HR4, HR4E, HR5E, which yielded 500 and 100 Å resolutions. Thermal gravimetric analysis (TGA) was measured using a TGA 2100 thermogravimetric analyzer (TA Instruments) to a heating rate of 10 °C/min. Differential scanning calorimetry (DSC) was conducted using a TA Instruments 2100 DSC with heating at 10 °C/min between 0 and 250 °C. The UV–Vis absorption spectra were recorded using a Cary 5000 UV–vis-near-IR double beam spectrophotometer. Cyclic voltammetry (CV) was performed using a PowerLab/AD instrument in a 0.1 M solution of tetrabutylammonium hexafluorophosphate (Bu_4NPF_6) in anhydrous acetonitrile as a supporting electrolyte at a scan rate of 50 mV/s. A glassy carbon disk (0.05 cm^2) coated with a thin polymer film, an Ag/AgCl electrode, and a platinum wire were used as the working electrode, reference electrode, and counter electrode, respectively. Density functional theory (DFT) calculations were performed at the B3LYP/6-31G* level of theory using the Spartan 08 computational programs. An Alpha-Step 500 profilometer was used to investigate the thickness of the spin-coated films. The atomic force microscope (AFM) (Multimode IIIa, Digital Instruments) was operated in the tapping mode to obtain surface images (surface area: 5 × 5 μm^2) under ambient conditions.

2.3.1. Fabrication and characterization of bulk heterojunction solar cells

The solar cell device was fabricated to a solution process except for two electrodes with a conventional structure of ITO-glass/PEDOT:PSS/BDT8TT:$PC_{71}BM$/Al. The indium tin oxide (ITO)-coated glass substrates were firstly cleaned by sonicating with detergents, DI–water, acetone, and isopropyl alcohol for 15 min each. And then the ITO–glass substrates were treated with UV-ozone treatments for 20 min. A hole extraction layer (ca. 40 nm) of PEDOT:PSS (Clevios P VP AI 4083, filtered at 0.45 μm PVDF) was spin-coated at 4000 rpm for 60 s onto the ITO substrates and baked at 120 °C for 20 min. The substrates were transferred into a nitrogen filled glove box. The photo-active layer (87 ± 1 nm) was prepared by spin-coating a bulk heterojunction blend solution of the BDT8TT and $PC_{71}BM$ in 1,2-dichlorobenzene with blend composition

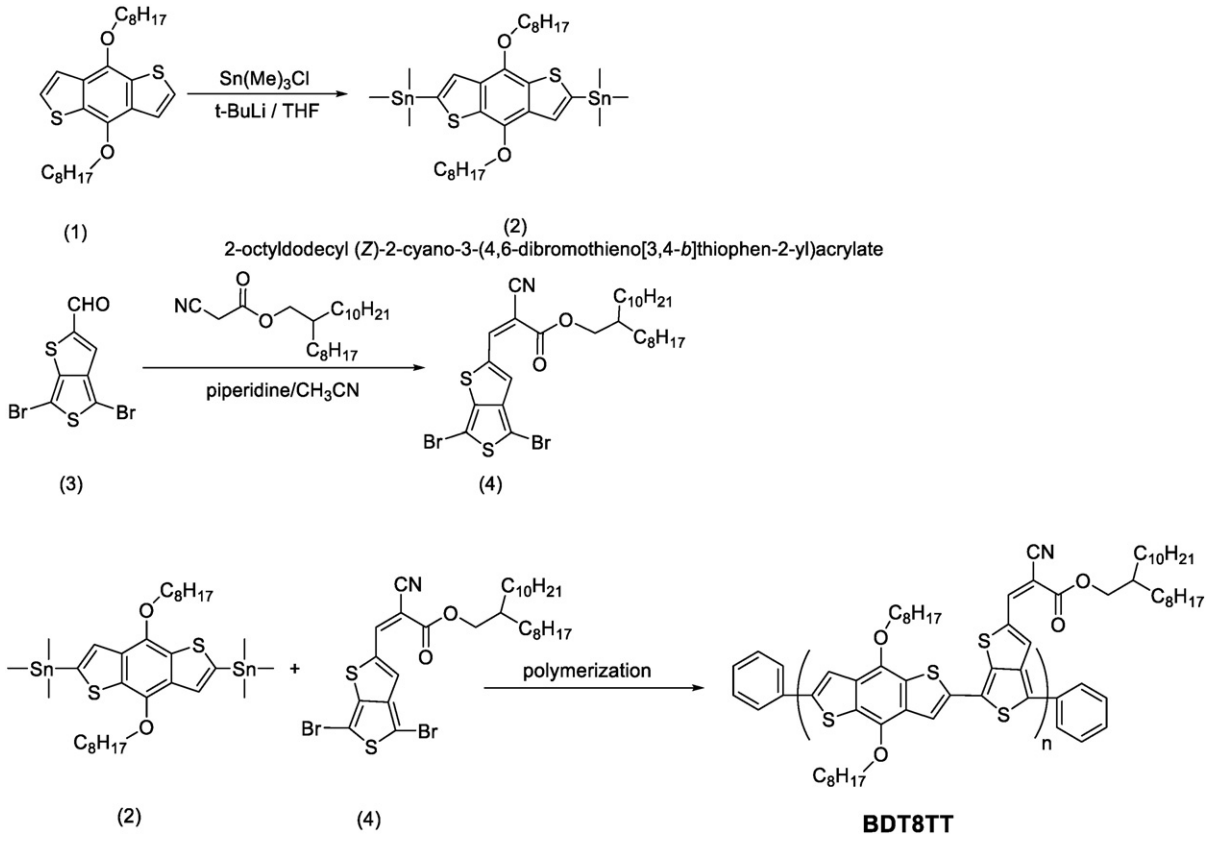

Scheme 1. Synthetic route for a conjugated polymer, BDT8TT.

of 1:1 to 1:4 *w*/*w* on the top of the ITO/PEDOT:PSS substrate. After that, a ca. 80 nm Al layer as a cathode electrode was deposited onto the photoactive layer through a shadow mask to define the active area of the devices (9 mm^2) under high vacuum of 2×10^{-6} Torr. The illuminated current density–voltage (*J*–*V*) characteristics of the solar cell devices were tested using a Keithley 2400 source measurement unit and an Oriel white light source under AM 1.5 conditions illuminated at 100 mW cm^{-2}. The external quantum efficiency (EQE) spectra were recorded using a photomodulation spectroscopic setup (model Merlin, Oriel), a calibrated Si UV detector, and a SR570 low noise current amplifier.

2.3.2. Fabrication and characterization of single carrier devices

We fabricated single charge carrier devices and investigated their hole and electron mobilities using space charge limited current (SCLC) method. The architecture of hole-only devices was glass/ITO/PEDOT:PSS/photoactive layer/Au (100 nm) and that of electron-only devices was Al (100 nm)/photoactive layer/Al (100 nm). The dark *J*–*V* characteristics of devices were measured under an applied forward bias. The carrier mobilities were extracted by fitting the *J*–*V* curves using the Mott–Gurney relationship.

$$J = \frac{9}{8}\varepsilon_0\varepsilon_r\mu_h\frac{V^2}{L^3}$$

where *J* is the dark current density, ε_0 is the permittivity of free space, ε_r is the relative dielectric constant of the transport medium, μ_h is the charge carrier mobility, *L* is the photoactive layer thickness and *V* is the internal voltage in the device ($V = V_{appl} - V_r - V_{bi}$, where V_{appl} is the applied voltage in the device, V_r is the voltage drop due to the

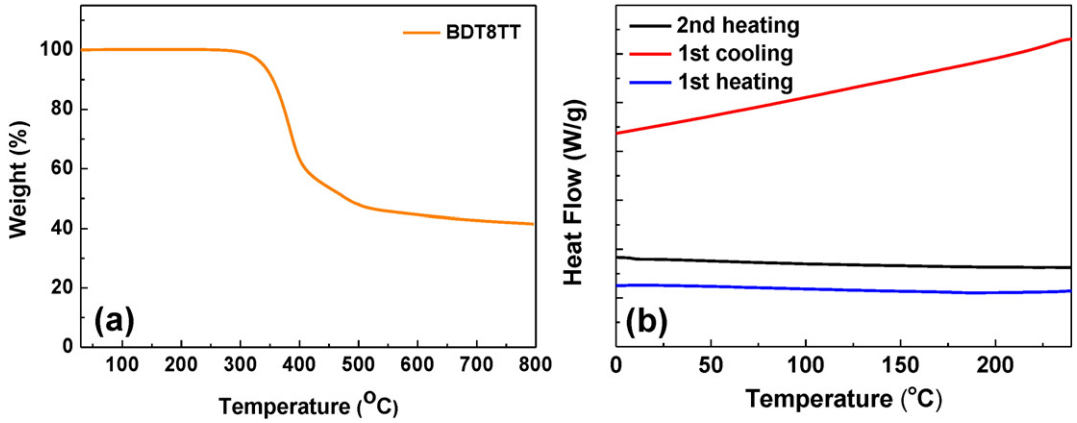

Fig. 1. TGA curve (a) and DSC trace (b) of the BDT8TT polymer with a heating rate of 10 °C min^{-1} under the protection of nitrogen.

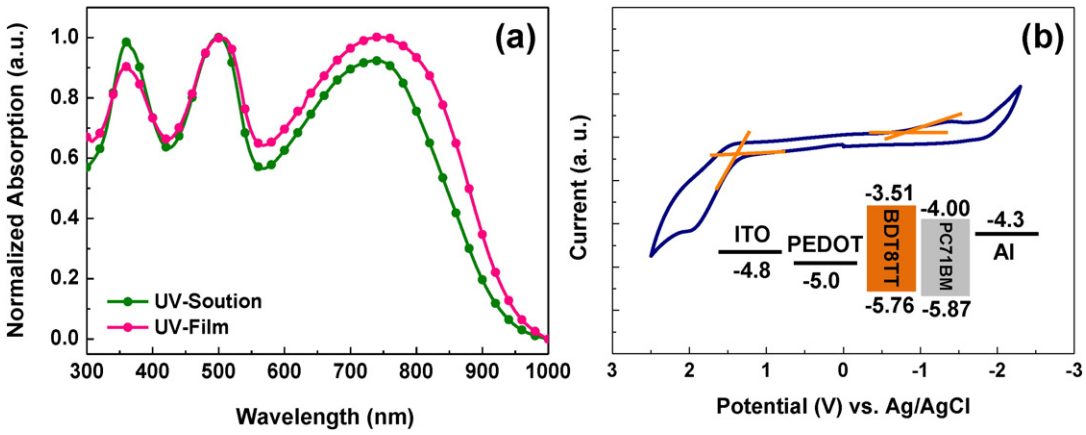

Fig. 2. Normalized UV–vis absorption spectra for BDT8TT in chloroform solution (green line) and thin solid films (pink line) (a) and cyclic voltammogram of BDT8TT films (b). The insert is schematic illustration of relative positions of energy levels for different components.

contact resistance and series resistance across the electrodes, and V_{bi} is the built-in voltage due to the relative work function difference between the two electrodes).

3. Results and discussion

3.1. Synthesis and characterization of the polymer

A new conjugated copolymer, BDT8TT was synthesized according to a Scheme 1. The (4,8-bis(octyloxy)benzo[1,2-b:4,5-b′]dithiophene-2,6-diyl)bis(trimethylstannane) monomer and 4,6-dibromothieno[3,4-b]thiophene-2-carbaldehyde monomer, which was synthesized through Knoevenagel reaction, were polymerized by Stille coupling reaction. The chemical structures of monomers and polymers were verified by ^{1}H-NMR, mass and IR. The number-average molecular weight (M_n) of BDT8TT was estimated by GPC technique, reaching 26,000 g mol^{-1} with a polydispersity index (PDI) of 1.9. The polymer was significantly soluble in common organic chlorinated solvents, such as 1,2-dichlorobenzene, chlorobenzene, chloroform and toluene owing to the long alkyl chain group [19].

The thermal properties of BDT8TT under a nitrogen atmosphere were characterized by TGA and DSC (Fig. 1). The TGA curve (Fig. 1a) revealed that the decomposition temperature (T_d, at a 5% weight loss) of the copolymer was 338 °C, implying that this conjugated polymer exhibited good thermal stability [20]. In the DSC trace (Fig. 1b), BDT8TT did not show any thermal transition up to 250 °C. From the thermal response, it can, therefore, be concluded that the BDT8TT is a quite low crystalline polymer against thermal stress [21].

3.2. Optical and electrochemical characteristics

The UV–vis absorption spectra of the synthesized polymer, BDT8TT, in chloroform solution and as thin solid film are shown in Fig. 2a, and the photophysical parameters are summarized in Table 1. First, the conjugated polymer had similar absorption spectra both in the solution and in the film, suggesting that similar π-stacked structures were formed in both solution and thin film states, which mainly resulted from the rigid units of benzodithiophene and thienothiophene [22–23].

In diluted chloroform solution, the polymer showed quite a broad absorption band to the near-IR region (near 1000 nm) with absorption maxima (λ_{max}) located at 361, 498, and 740 nm. Through this strong light absorption in the visible to near IR region, we can expect that BDT8TT polymer generates considerable light harvesting favorable to high photocurrents. Relative to the solution absorption, as mentioned above, the absorption spectrum of the polymer solid film was almost unchanged. However, the film for BDT8TT exhibited a broaden absorption band with the red-shifted λ_{max} of ca. 10 nm. This indicates that the BDT8TT compound provides better intermolecular interaction and aggregation in the solid state [24]. The optical band gap (E_g) calculated from the absorption edge (961 nm) of the thin solid film, was 1.29, which is a quite low optical band gap.

The highest occupied molecular orbital (HOMO) and lowest unoccupied molecular orbital (LUMO) levels of the BDT8TT polymer were evaluated by cyclic voltammetry (CV), and the results are shown in Fig. 2b. The HOMO and LUMO levels of the target polymer could be deduced from the oxidation and reduction onsets, respectively, assuming that the energy level of ferrocene (Fc) was 4.8 eV below the vacuum level [25]. The oxidation and reduction onset potentials of BDT8TT were 1.40 and −0.53 V, respectively, which corresponded to the potential of −5.76 eV for HOMO and −3.51 eV for LUMO energy (Table 1). From the CV measurement results, we concluded that newly synthesized BDT8TT polymer shows a considerably deeper HOMO energy level compared to previously reported CNTT polymer (−5.32 eV). We argue that the introduction of BDT units with relatively weak electron-donating ability could lead to the modification of energy levels, resulting in low-lying HOMO levels. This argument will be further examined by the theoretical calculations discussed below.

In general, the polymer exhibits extremely deep HOMO energy levels (below −5.50 eV), which implies that this polymer could be very stable against oxidization, hence leading to high device stability

Table 1
Photophysical and electrochemical properties of a conjugated BDT8TT polymer.

Polymer	T_d (°C)[a]	λ_{max} (nm) solution	λ_{max} (nm) film	E_{onset}^{ox} (eV)	E_{onset}^{red} (eV)	E_{HOMO} (eV)	E_{LUMO} (eV)
BDT8TT	338	361, 498, 740	360, 501, 748	1.40	−0.85	−5.76	−3.51

[a] Decomposition temperature corresponding to 5% weight loss in N_2 determined by TGA.

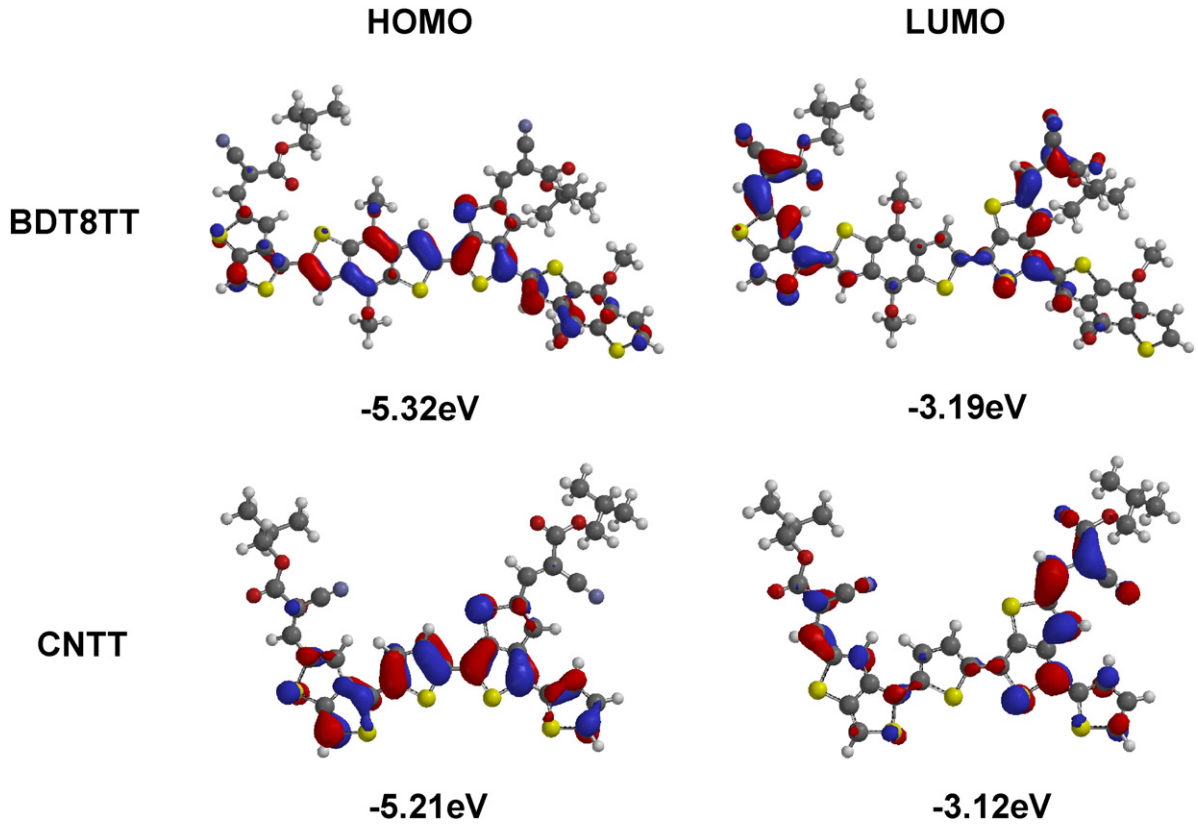

Fig. 3. Representations of the BDT8TT and CNTT dimer HOMO and LUMO as obtained at the B3LYP/6-31G* level of theory.

[26]. Furthermore, this deep HOMO level of the BDT8TT means a higher Voc could be expected because Voc is linearly correlated with the difference of the HOMO of the donor and the LUMO of the acceptor ($PC_{71}BM$, −4.00 eV) (see insert Fig. 2b) [27].

3.3. DFT electronic structure calculations

The electron state density of the polymer was investigated by performing theoretical calculations using density functional theory (DFT) to model the compounds. The DFT-computed frontier orbitals of the BDT8TT dimers are shown in Fig. 3. Methyl alkyl groups were used in place of the bulky alkyl substituents to limit computation time, since they do not significantly affect the equilibrium geometry or thus, the electronic properties [28]. As shown in Fig. 3, the HOMO was delocalized over the polymer backbone, whereas the LUMO was mostly localized on the cyano acrylate unit due to the electron deficient property [12]. Moreover, the computed HOMO and LUMO values showed −5.32 eV and −3.19 eV, respectively.

Furthermore, in order to clarify the correlation between the change in energy state density and electron-donating units in the polymer backbone, DFT calculations of CNTT compounds were also investigated. The computed HOMO and LUMO levels of CNTT dimers exhibited

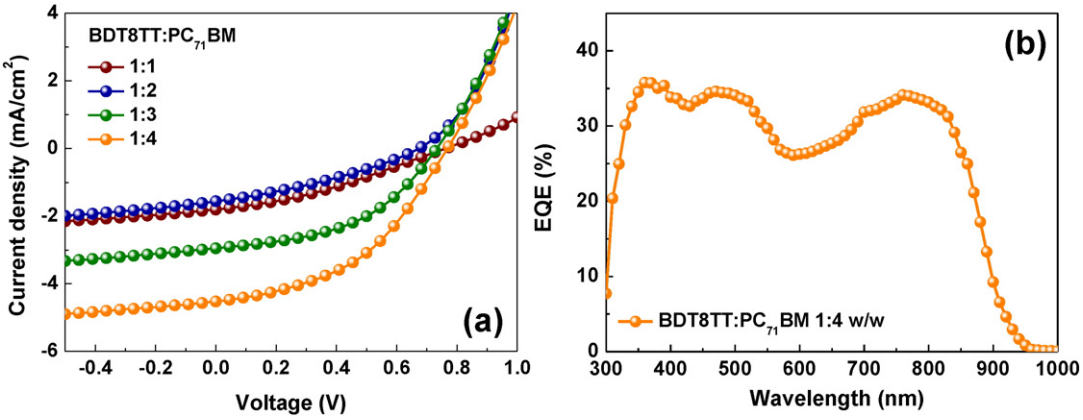

Fig. 4. (a) The *J–V* characteristics of polymer solar cells based on BDT8TT:$PC_{71}BM$ under the illumination of AM 1.5G, 100 mW cm^{-2} and (b) the EQE curve of the corresponding 1:4 *w/w* device.

Table 2
Photovoltaic performances of the bulk heterojunction BDT8TT:$PC_{71}BM$ solar cells under various donor:acceptor blend weight ratios.

Active layer	Blend ratios	*Voc* (V)	*Jsc* (mA/cm^2)	FF (%)	PCE (%)
BDT8TT:$PC_{71}BM$	1:1	0.75	1.8	32.9	0.40
	1:2	0.74	3.0	42.6	0.96
	1:3	0.73	3.2	46.7	1.01
	1:4	0.77	4.5	47.3	1.63

−5.21 eV and −3.12 eV, respectively. These findings indicate that the BDT8TT clearly showed deeper HOMO energy compared to CNTT polymer in these DFT results, consistent with CV analysis.

3.4. Solar cell properties

We investigated the photovoltaic properties of the copolymer in BHJ solar cells having a sandwich structure, ITO/PEDOT:PSS/BDT8TT:$PC_{71}BM$/Al. The OPVs were fabricated by the spin-casting of *o*-dichlorobenzene (*o*-DCB) solutions of BDT8TT/$PC_{71}BM$ blends. The blend ratio was an important factor that influenced the device performance [29]; therefore, we carefully tuned the blend ratio of the active layers between a ratio of 1:1 and 1:4 (*w*/*w*), polymer:$PC_{71}BM$. Typical *J*–*V* characteristics of devices with the different blend composition under AM 1.5G irradiation are depicted in Fig. 4a. And detailed device parameters (Voc, *J*sc, FF and PCE) are summarized in Table 2.

The BDT8TT:$PC_{71}BM$ solar cell with a 1:1 blend ratio showed very low device performance of 0.4% efficiency with a Voc of 0.75 V, a *J*sc of 1.8 mA cm^{-2}, and a FF of 32.9%. However, an increase in fill factors (to ca. 43–47%) was coupled with a dramatic increase in photocurrent densities (*J*scs) to 3.0 mA cm^{-2} for devices with both 1:2 and 1:3 blend conditions, and thus the PCEs exhibited 0.96% for the 1:2 device and 1.0% for the 1:3 device, respectively. Notably, the FF and *J*sc values are affected by $PC_{71}BM$ concentration in the blend. Interestingly, further enhanced PCE of 1.5% with a Voc of 0.77 V, a *J*sc of 4.5 mA cm^{-2} and an FF of 44.2% were obtained in the device with BDT8TT:$PC_{71}BM$ 1:4 layers, which is the highest value in this system.

Above all things, indeed, our experiments results display that BDT8TT has much higher open circuit voltage value than that of the CNTT polymer (0.38 V). This is in good agreement with our synthesis strategy and results from the CV and DFT study, in which BDT8TT exhibited a significantly lower HOMO level than that ofCNTT.

To investigate the spectral photocurrent response of the devices, external quantum efficiency (EQE) spectrum was collected. As shown in Fig. 4b, 1:4 *w*/*w* devices showed a relatively high photo-conversion efficiency over the whole wavelength range of 300–1000 nm. In addition, the EQE spectrum agreed well with the optical absorption curve and a close correlation with the photocurrent [30].

3.5. Morphology results

The morphology of the photoactive layer plays an important role in the photovoltaic performance of solar cells along with other photophysical properties and in several situations the device performance strongly depends on its morphological features. To explore the changes of blend compositions on the morphology and device performance of BDT8TT:$PC_{71}BM$ film, we observed the surface morphologies of the blend films using atomic force microscopy (AFM). Fig. 5 shows a topography nanoscale image of the BDT8TT:$PC_{71}BM$ blend films with different blend ratios.

According to the AFM images, all blend films showed quite homogeneous and uniform surface morphologies. Notably, however, increasing the $PC_{71}BM$ content to the weight ratio in the active blends, results in more aggregated surfaces with larger-scale domains. This relatively coarse surface and more phase-separated aggregation are beneficial to the charge transportation, thereby leading to an increase in J_{SC} and FF as well as the device efficiency [31–32].

Furthermore, as the amount of $PC_{71}BM$ increased from 1:1 to 1:4, the root mean-square roughness (rms) values for the blend films also gradually increased to 0.75, 1.01, 1.89 and 2.23 nm at ratios of 1:1, 1:2, 1:3 and 1:4, respectively. This finding suggests that a higher surface roughness is expected to increase the internal light scattering and enhance light absorption [33]. Therefore, these two advantageous characteristics of 1:4 *w*/*w* blend films were expected to enhance the J_{SC} and FF values with higher efficiency of BDT8TT:$PC_{71}BM$ devices relative to the device with 1:1, 1:2 or 1:3 active blend ratios.

3.6. Charge carrier transport characteristics

We used SCLC measurements to investigate the charge carrier transport in the BDT8TT:$PC_{71}BM$ blend devices toward a better understanding of the photovoltaic properties. Hole-only devices with the structure of glass/ITO/PEDOT:PSS/photoactive layer/Au and electron-only devices with the architecture of Al/photoactive layer/Al were fabricated and characterized. The dark *J*–*V* characteristics of both hole-only and electron-only diodes can be well fitted to the Mott-Gurney relation, which are shown in Fig. 6. The hole mobility (μ_h) of BDT8TT:$PC_{71}BM$ with 1:1 *w*/w appears 1.02×10^{-4} cm^2/Vs, whereas that of 1:4 blend ratio films shows 4.25×10^{-4} cm^2/Vs. This result suggests that the higher carrier mobility in BDT8TT:$PC_{71}BM$ with 1:4 *w*/*w* blend composition is due to the denser packing of the polymers [34], which consistent with the results of AFM data. The electron mobility (μ_e) also exhibits same trend with hole carrier mobility (6.38×10^{-6} cm^2/Vs for 1:1 *w*/*w* blend films and 7.17×10^{-5} cm^2/Vs for 1:4 *w*/*w* blend films). The ratio (μ_h/μ_e) between the hole and electron mobilities from 15.98 to 5.92 (1:1 *w*/*w* to 1:4 *w*/*w*), which indicates a more balanced charge transport in the device based on BDT8TT:$PC_{71}BM$ with the 1:4 blend composition. The balance charge carrier mobility within the active layer resulted in high J_{SC} and FF because the accumulated SCLC charges,

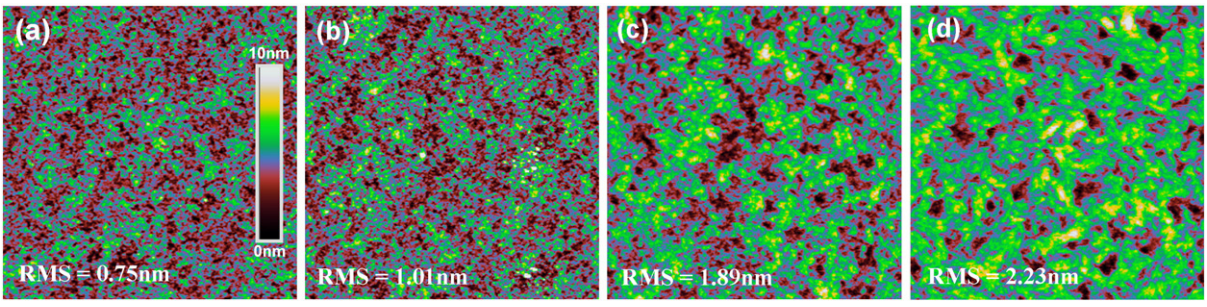

Fig. 5. AFM height images of BDT8TT:$PC_{71}BM$ bulk heterojunction films with different blend composition: (a) 1:1, (b) 1:2, (c) 1:3 and (d) 1:4 *w*/*w*.

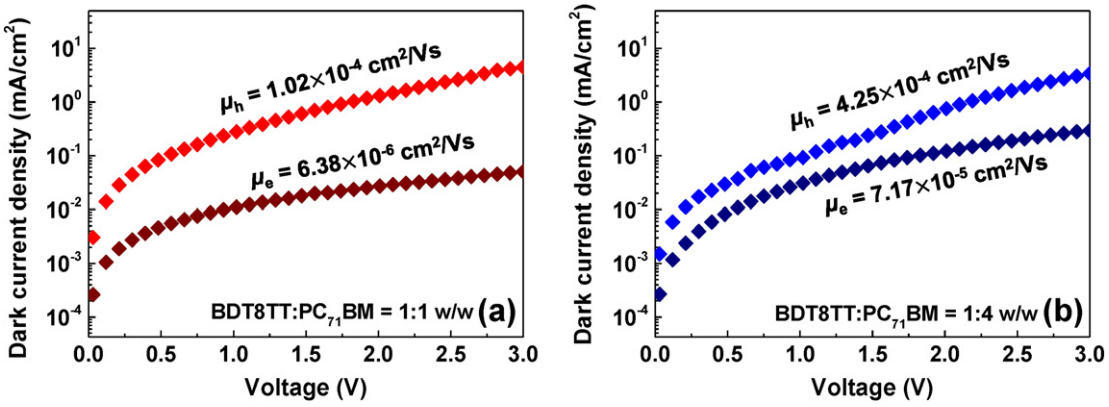

Fig. 6. Dark current–voltage (*J*–*V*) characteristics of hole-only and electron-only devices for BDT8TT:$PC_{71}BM$ blends with (a) 1:1 *w*/*w* blend ratio and (b) 1:4 *w*/*w* blend composition.

and hence the recombination processes, are reduced by the increase in carrier mobility and enhancement in charge collection efficiency [35].

4. Conclusion

In conclusion, a new conjugated polymer, BDT8TT, containing benzodithiophene and thienothiophene-flanked cyano acrylate side chain has been designed and synthesized. The copolymer demonstrates good solubility in common organic chlorinated solvents, excellent thermal stability (T_d > 338 °C), quite broad absorption, and a highly deep HOMO energy level at −5.76 eV. The polymer solar cell fabricated from the blend of BDT8TT:$PC_{71}BM$ exhibited a moderate PCE with a high Voc of 0.77 V. This result suggests the potential to replace thiophene unit with benzodithiophene moiety in the design and synthesis of semiconducting polymers with efficient solar cell performance and, especially, to lower the HOMO energy levels of the conjugated polymers, thereby, boosting the open circuit voltage of solar cell devices.

Acknowledgments

This research was supported by Nano-Material Technolgy Development Program through the National Research Foundation of NRF funded by Korean Government (2010-0029084) and New & Renewable Energy of the KETEP grant funded by the Korea Government Ministry of Knowledge Economy (20123010010140).

References

[1] G. Yu, J. Hummelen, F. Wudl, A.J. Heeger, Polymer photovoltaic cells: enhanced efficiencies via a network of internal donor–acceptor heterojunctions, Science 270 (1995) 1789–1791.
[2] S. Gunes, H. Neugebauer, N.S. Sariciftci, Conjugated polymer-based organic solar cells, Chem. Rev. 107 (2007) 1324–1338.
[3] Y.-J. Cheng, S.–.H. Yang, C.–.S. Hsu, Synthesis of conjugated polymers for organic solar cell applications, Chem. Rev. 109 (2009) 5868–5923.
[4] G. Li, R. Zhu, Y. Yang, Polymer solar cells, Nat. Photonics 6 (2012) 153–161.
[5] C.–.C. Chen, W.–.H. Chang, K. Yoshimura, K. Ohya, J. You, J. Gao, Z. Hong, Y. Yang, An efficient triple-junction polymer solar cell having a power conversion efficiency exceeding 11%, Adv. Mater. 26 (2014) 5670–5677.
[6] L. Huo, T. Liu, X. Sun, Y. Cai, A.J. Heeger, Y. Sun, Single-junction organic solar cells based on a novel wide-bandgap polymer with efficiency of 9.7%, Adv. Mater. 27 (2015) 2938–2944.
[7] J.–.S. Wu, S.–.W. Cheng, Y.–.J. Cheng, C.–.S. Hsu, Donor–acceptor conjugated polymers based on multifused ladder-type arenes for organic solar cells, Chem. Soc. Rev. 44 (2015) 1113–1154.
[8] T. Xu, L. Yu, How to design low bandgap polymers for highly efficient organic solar cells, Mater. Today 17 (2014) 11–15.
[9] C. Cui, W.–.Y. Wong, Y. Li, Improvement of open-circuit voltage and photovoltaic properties of 2D-conjugated polymers by alkylthio substitution, Energy Environ. Sci. 7 (2014) 2276–2284.
[10] T. Ma, K. Jiang, S. Chen, H. Hu, H. Lin, Z. Li, J. Zhao, Y. Liu, Y.–.M. Chang, C.–.C. Hsiao, H. Yan, Efficient low-bandgap polymer solar cells with high open-circuit voltage and good stability, Adv. Energy Mater. 5 (2015) 1501282.
[11] Q. Liu, X. Bao, L. Han, C. Gu, M. Qiu, Z. Du, R. Sheng, M. Sun, R. Yang, Improved open-circuit voltage of benzodithiophene based polymer solar cells using bulky terthiophene side group, Sol. Energy Mater. Sol. Cells 138 (2015) 26.
[12] X. Liu, Y.J. Kim, M–.J. Kim, C.E. Park, Y.–.H. Kim, A unique concept of copolymer composed of main chain donor and side chain acceptor for promising bulk heterojunction solar cells, Synthetic Metals 205 (2015) 195–200.
[13] X. Yang, A. Uddin, Retraction notice to "effect of thermal annealing on P3HT:PCBM bulk-heterojunction organic solar cells: a critical review", Renew. Sust. Energ. Rev. 30 (2014) 324–336.
[14] L. Ye, S. Zhang, L. Huo, M. Zhang, J. Hou, Molecular design toward highly efficient photovoltaic polymers based on two-dimensional conjugated benzodithiophene, Acc. Chem. Res. 47 (2014) 1595–1603.
[15] H.–.J. Wang, C.–.P. Chen, R.–.J. Jeng, Polythiophenes comprising conjugated pendants for polymer solar cells: a review, Materials 7 (2014) 2411–2439.
[16] H. Zhou, L. Yang, W. You, Rational design of high performance conjugated polymers for organic solar cells, Macromolecules 45 (2012) 607–632.
[17] D. Liu, W. Zhao, S. Zhang, L. Ye, Z. Zheng, Y. Cui, Y. Chen, J. Hou, Highly efficient photovoltaic polymers based on benzodithiophene and quinoxaline with deeper HOMO levels, Macromolecules 48 (2015) 5172–5178.
[18] J.H. Park, Y.G. Seo, D.H. Yoon, Y.–.S. Lee, S.–.H. Lee, M. Pyo, K. Zong, A concise synthesis and electrochemical behavior of functionalized poly(thieno[3,4-*b*]thiophenes): new conjugated polymers with low bandgap, Eur. Polym. J. 46 (2010) 1790–1795.
[19] H. Li, T. Earmme, S. Subramaniyan, S.A. Jenekhe, Bis(naphthalene imide)diphenylanthrazolines: a new class of electron acceptors for efficient nonfullerene organic solar cells and applicable to multiple donor polymers, Adv. Energy Mater. 5 (2015) 1402041.
[20] L. Chen, P. Shen, Z.–.G. Zhang, Y. Li, Side-chain engineering of benzodithiophene-thiophene copolymers with conjugated side chains containing the electron-withdrawing ethylrhodanine group, J. Mater. Chem. A 3 (2015) 12005–12015.
[21] Y.J. Kim, Y.R. Cheon, J.–.W. Jang, Y.–.H. Kim, C.E. Park, A potential naphtha[2,1-*b*:3,4-*b*′]dithiophene-based polymer with large open circuit voltage for efficient use in organic solar cells, J. Mater. Chem. C. 3 (2015) 1904–1912.
[22] L. Lu, W. Chen, T. Xu, L. Yu, High-performance ternary blend polymer solar cells involving both energy transfer and hole relay processes, Nat. Commun. 6 (2015) 7327.
[23] C. Duan, A. Furlan, J.J. van Franeker, R.E.M. Willems, M.M. Wienk, R.A.J. Janssen, Wide-bandgap benzodithiophene–benzothiadiazole copolymers for highly efficient multijunction polymer solar cells, Adv. Mater. 27 (2015) 4461–4468.
[24] H. Kang, S.Y. An, B. Walker, S. Song, T. Kim, J.Y. Kim, C. Yang, Thienoisoindigo(TIIG)-based small molecules for the understanding of structure–property–device performance correlations, J. Mater. Chem. A 3 (2015) 9899–9908.
[25] Y.R. Cheon, Y.J. Kim, J.–j. Ha, M–.J. Kim, C.E. Park, Y.–.H. Kim, TPD-based copolymers with strong interchain aggregation and high hole mobility for efficient bulk heterojunction solar cells, Macromolecules 47 (2014) 8570–8577.
[26] W.–.H. Tseng, H.–.C. Chen, Y.–.C. Chien, C.–.C. Liu, Y.–.K. Peng, Y.–.S. Wu, J.–.H. Chang, S.–.H. Lium, S.–.W. Chou, C.–.L. Liu, Y.–.H. Chen, C. Wu, P.–.T. Chou, Comprehensive study of medium-bandgap conjugated polymer merging a fluorinated quinoxaline with branched side chains for highly efficient and air-stable polymer solar cells, J. Mater. Chem. A 2 (2014) 20203–20212.
[27] X. Guo, N. Zhou, S.J. Lou, J. Smith, D.B. Tice, J.W. Hennek, R.P. Ortiz, J.T.L. Navarrete, S. Li, J. Strzalka, L.X. Chen, R.P.H. Chang, A. Facchetti, T.J. Marks, Polymer solar cells with enhanced fill factors, Nat. Photonics 7 (2013) 825–833.
[28] J. Ku, S. Song, S.H. Park, K. Lee, H. Suh, Y. Lansac, Y.H. Jang, Palladium-assisted reaction of 2,2-diakylbenzimidazole and its implication on organic solar cell performances, J. Phys. Chem. C 119 (2015) 14063.
[29] S.H. Park, A. Roy, S. Beaupre, S. Cho, N. Coates, J.S. Moon, D. Moses, M. Leclerc, K. Lee, A.J. Heeger, Bulk heterojunction solar cells with internal quantum efficiency approaching 100%, Nat. Photonics 3 (2009) 297–302.
[30] Z. He, C. Zhong, Su S, M. Xu, H. Wu, Y. Cao, Enhanced power-conversion efficiency in polymer solar cells using an inverted device structure, Nat. Photonics 6 (2012) 591–595.

[31] W. Huang, E. Gann, L. Thomsen, C. Dong, Y.–.B. Cheng, C.R. McNeill, Unraveling the morphology of high efficiency polymer solar cells based on the donor polymer PBDTTT-EFT, Adv. Energy Mater. 5 (2015) (1401259).
[32] C. Dyer-Smith, I.A. Howard, C. Cabanetos, A.E. Labban, P.M. Beaujuge, F. Laquai, Interplay between side chain pattern, polymer aggregation, and charge carrier dynamics in PBDTTPD:PCBM bulk-heterojunction solar cells, Adv. Energy Mater. 5 (2015) 1401778.
[33] L. Lan, G. Zhang, Y. Dong, L. Ying, F. Huang, Y. Cao, Novel medium band gap conjugated polymers based on naphtha[1,2-c:5,6-c]bis[1,2,3]triazole for polymer solar cells, Polymer 67 (2015) 40–46.
[34] K.H. Park, Y.J. Kim, G.B. Lee, T.K. An, C.E. Park, S.–.K. Kwon, Y.–.H. Kim, Recently advanced polymer materials containing dithieno[3,2-*b*:2′,3′-*d*]phosphole oxide for efficient charge transfer in high-performance solar cells, Adv. Funct. Mater. 25 (2015) 3991–3997.
[35] J. Fischer, J. Widmer, H. Kleemann, W. Tress, C. Koerner, M. Riede, K. Vandewal, K. Leo, A charge carrier transport model for donor-acceptor blend layers, J. Appl. Phys. 117 (2015) 045501.